Numerical Simulation of a cost efficient novel CPVT solar collector

Daniel Santos[1], Jesús Castro[1], Deniz Kizildag[1], Joaquim Rigola[1] and Assensi Oliva[1]

[1]Heat and Mass Transfer Technological Center, Terrassa (Spain)

Abstract

In this work, the simulation of a Concentrated PhotoVoltaic Thermal (CPVT) solar collector system has been done by means of Finite Volume Method. The system consists of a parabolic collector, which concentrates solar irradiance onto solar cells, which are refrigerated attaching them to a pipe which contains water. At the same time, this water is warmed up. Numerical results are compared with experimental data both obtained within the current eranet project for the Economic COgeneration by Efficiently COncentrated SUNlight (ECOSUN). The idea of this project is to study how to take advantage of the residual heat produced by the photovoltaic elements. Warming up water is proposed as a possibility, due to the synergy obtained because water refrigerates the whole system. First numerical results show a reasonable agreement against experimental data. The CPVT model of this project is oriented to optimize the design for solar cooling applications. Finally, new pipe geometries including fines are purposed in order to increase the thermal heat exchange between the CPVT solar collector and the water.

Keywords: parabolic collector, solar energy, solar power, solar cell, FVM, CPVT.

1. Introduction

Solar cell technology combines knowledge of different areas, such as physic of materials and thermal engineering. One powerful tool that allows us to obtain better analysis of a solar cell system and help us in the optimizing process is Computational Fluid Dynamics (CFD) (Guadamund, et al.). This field of knowledge takes charge solving (numerically) the equations that govern the physics involved in the physics of fluids and heat and mass transfer, allowing us to simulate different configurations of physical systems, such as the ones involving solar energy.

The purpose of this project is focused on concentrated photovoltaic thermal collector (CPVT), which concentrates solar irradiance onto a row of photovoltaic solar cells (Sharaf and Orhan). At the same time, these solar cells must be refrigerated in order to work optimally. This could be done, for instance, attaching these solar cells to a pipe which contains some fluid (water in our case). Furthermore, this residual heat could be used to warm up this fluid. ECOSun project has as main objective of cost reduction of electricity and heat co-generation via a Concentrated Photovoltaic/Thermal (CPV-T) system by applying low-cost materials and advanced industrial manufacturing methods. In the CPV-T system, the solar radiation is captured in parabolic through concentrator based on a novel support structure fabricated by injection moulding and focused on a Co-Generation Absorber Module (CAM), where special c-SiPV-cells are operated under concentration. One of the subtasks of the project has been to simulate properly the whole CPVT system, comparing our results against the results obtained experimentally. Different configurations of inflow water will be taken into account, using a closed system with a glass envelope and low-pressure air. The whole CPVT system can be attached to absorption machines in order to take advantage of the residual heat (Castro et al.).

By means of experimental data, the CFD analysis is able to model all heat transfer processes reproducing the whole phenomena not only for validation purposes by means of experimental data comparison and physical models' calibrations, but also to simulate different system conditions, avoiding the necessity of repeating an experiment for such conditions. In this regard, we can obtain new results for different materials or configurations of the pipe, including shape and the possibility of having fins.

doi:10.18086/swc.2021.22.08 Available at http://proceedings.ises.org

2. Numerical Model and Implementation

The CPVT solar cell system, illustrated in Figure 1, can be physically decomposed into three parts: solid regions, fluid domains and coupling interfaces. In the following list, the equations to be solved in each region are shown.

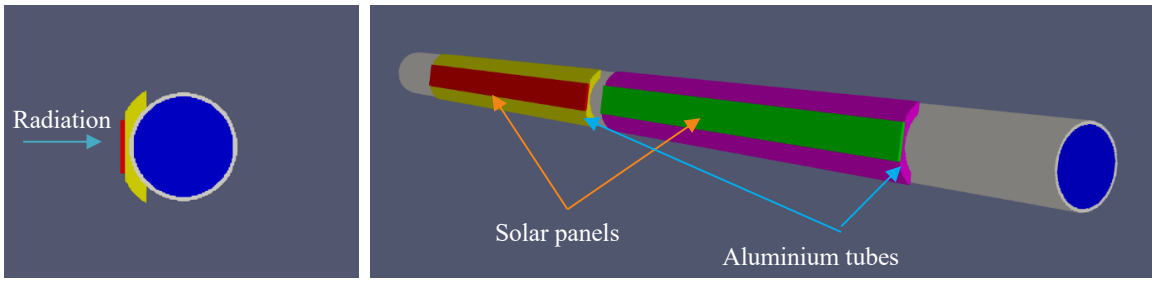

Fig. 1: CPVT cross section configuration (left); CPVT configuration front of parabolic collector (collector not included)

- Solid elements: energy equation conservation, (note that for this case, the velocities are equal to 0).

$$\frac{\partial T}{\partial t} + \boldsymbol{u} \cdot \nabla \mathrm{T} = \frac{k}{\rho c_p} \nabla^2 \boldsymbol{T} + \frac{\boldsymbol{J}}{\rho c_p}, \qquad \text{(eq. 1)}$$

where T is the temperature, **u** is the velocity (**u**=0 for solid elements), k is the thermal conductivity, ρ is the density, c_p is the heat capacity and J is the source term.

- Fluid elements: (Eq.1) + Incompressible Navier-Stokes equations with buoyancy term (Boussinesq approximation):

$$\nabla \cdot \boldsymbol{u} = 0, \qquad \text{(eq. 2)}$$

$$\frac{\partial \boldsymbol{u}}{\partial t} + (\boldsymbol{u} \cdot \nabla)\mathbf{u} = -\frac{1}{\rho}\nabla(p - \rho \boldsymbol{g} \cdot \boldsymbol{z}) + \nu \nabla^2 \boldsymbol{u} - \boldsymbol{g}\beta(T - T_0), \qquad \text{(eq. 3)}$$

where **u** is the velocity, p is the pressure, ρ is the density, ν is the kinematic viscosity, **g** is the gravity constant, β is the thermal expansion coefficient, and T is the temperature.

- Coupling interfaces (solid-solid and fluid-solid):
  - Heat flux exiting one domain enters the other: $Q_1 = -Q_2$.
  - Same temperature at the interface: $T_1 = T_2$.

The heat flux is computed taking into account convective and radiative terms. Natural convection is found in the surrounding air, while forced convection can be found between the fluid and the pipe. The radiation model used is the Finite Volume Discrete Ordinates Method, which solves the RTE (Radiative Transfer Equation):

$$\hat{\boldsymbol{s}} \cdot \nabla I(\boldsymbol{r}, \hat{\boldsymbol{s}}) = \kappa I_b + (\kappa + \sigma_s) I, \qquad \text{(eq. 4)}$$

applying a finite volume method (Colomer, 2006; Wang, 2020). In the previous equation, the intensity radiation field I is solved, which is defined as the energy due to radiation, propagating along a given direction $\hat{\boldsymbol{s}}$, that crosses a unit area normal to $\hat{\boldsymbol{s}}$, per unit area, unit solid angle around $\hat{\boldsymbol{s}}$, unit wavelength and time. The absorption coefficient κ and the scattering coefficient σ_s model the medium behavior.

Finally, the radiation coming from the parabolic collector is assumed as a radiative boundary condition computed as (Zarza, 2015):

$$q = \frac{W_{par}}{W_{pV}} G_b \eta_{opt}, \qquad \text{(eq. 5)}$$

where W_{par} is the aperture width of the parabola, W_{pV} is the height of the solar cells, G_b is the direct solar irradiance and η_{opt} is the optical efficiency of the parabola.

In order to perform simulations of the experiments, a software that has allowed to simulate conjugate heat transfer equations has been required. Furthermore, radiation must also be solved. OpenFOAM code (OF) has been chosen to do this particular task. The solver selected from OF library has been "chtMultiRegionFoam". This is a transient solver capable to deal with conjugate heat transfer between solid and fluid regions. Besides, radiation can be added to the solver too. Regarding radiation models, OF code has three integrated models: surface-to-surface model (or view factors model), P1 and fvDOM. Last one has been chosen for the sake of being the more precise model.

3. CPVT Simulation

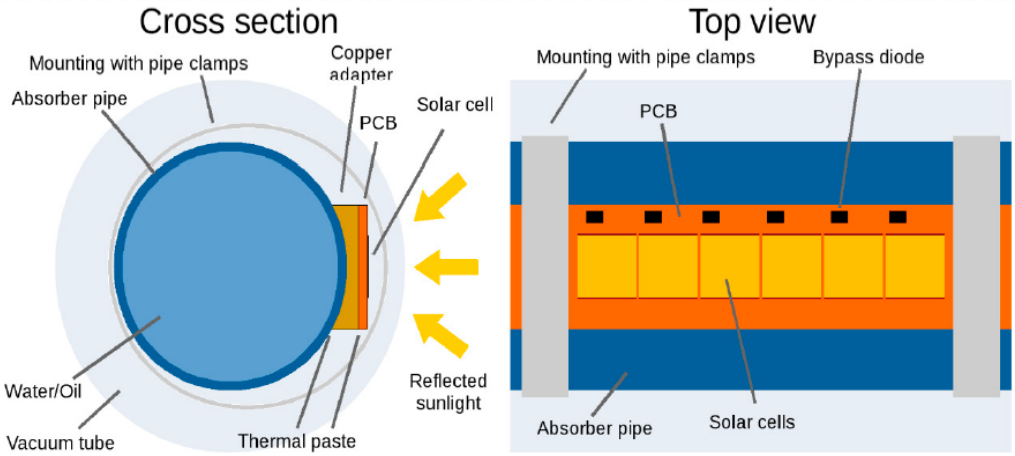

Fig. 2: CPVT solar collector experimental configuration scheme (collector not included) (Felsberger, et. al. 2020)

As we can see in Figure 2 from a general point view, important components of the system to take into account are the following ones: i) an absorber pipe; ii) a printed circuit board (PCB) which have the solar cells attached; and iii) a piece which connects the PCB with the pipe and an envelope glass to isolate the system. Furthermore, a parabolic solar collector is used to concentrate solar power onto the solar cells. Finally, an envelope glass (100mm diameter) is used to cover our system with a low-pressure air.

Radiation is coming from the parabolic collector and enters in the system, while PCB is heating up, water is flowing from left to right absorbing heat and cooling the solar cells.

3.1 Numerical verification and detailed validation

The model has been numerically verified and experimentally validated using data coming from EcoSUN experimental test cases under lab tests conditions (Felsberger, et. al. 2020; Buchroithner, et al.). These experiments consisted of a single CPV cell which received controlled radiation guided by a tunnel. This cell was attached to a pipe using a piece of copper. The pipe contained water flowing which refrigerated our system. Figure 3 shows a schematic picture of the experiment. A temperature sensor was located behind the CPV cell.

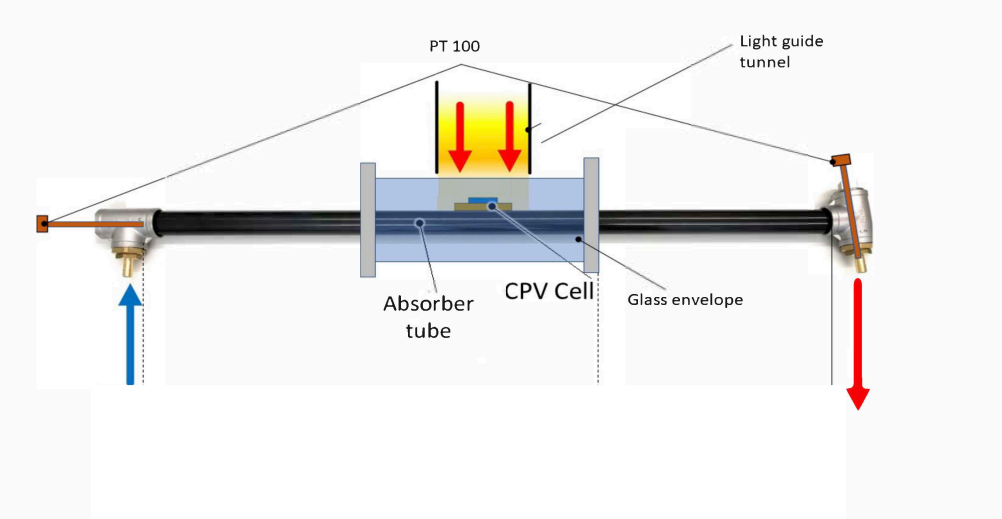

Fig. 3: CPVT single solar collector experimental configuration (Felsberger, et al. 2020; Buchroithner, et al.).

The main purpose of this model was to reproduce properly the temperature reached by the system in the steady state. In figure 4, the temperature obtained numerically with our model is shown, along with the steady state temperatures obtained in the experiments. In both cases, numerically and experimentally, temperatures were between 33-34ºC in the sensors. Numerical results on outlet fluid water temperature and different solid temperature points along the conduct present a very good agreement with an error lower than 3% in all cases. Once our model has been tested, we can advance to the next step: the simulation of a full CPVT solar collector. Even though we have tested the physical model, its robustness will be tested again against experimental data of the CPVT solar collector experiment.

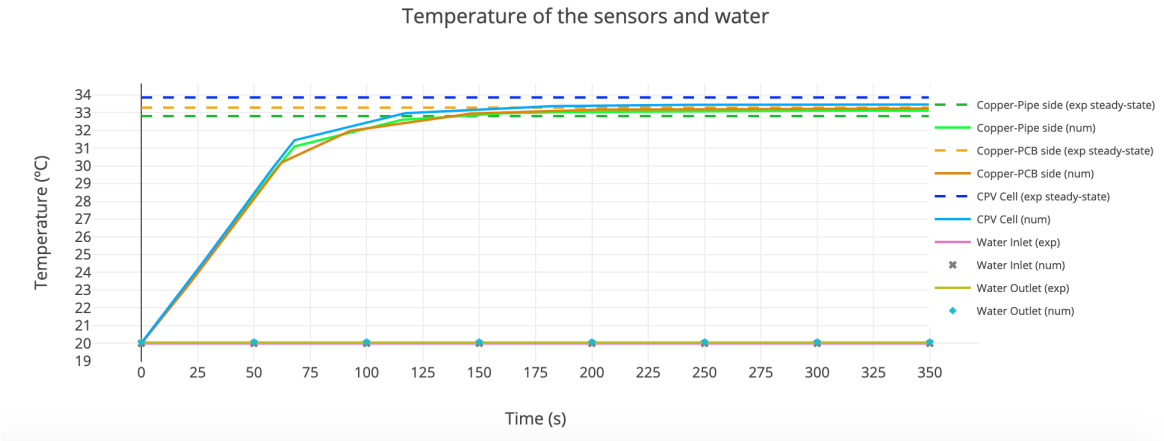

Fig. 4: Temperature obtained at temperature sensors. Water input temperature is 20.0ºC. Slashed lines represent the steady state temperature found in the experiments.

3.2 Numerical test cases under real working conditions

Different tests have been done within this configuration in order to obtain experimental data (Felsberger, et. al. 2021). The main test consisted of three experiments with different irradiances (DNI) and different heat transfer fluid (HTF) temperature. These experiments were carried out with a glass envelope of 3mm thickness, an HTF flow rate about 11 L/min.

The first one had an HTF temperature of 17ºC and a DNI of 780 W/m2, the second one an HTF of 65ºC and a DNI of 750 W/m2 and the last one had an HTF of 90ºC and a DNI of 650 W/m2. Again, the objective is to reproduce properly the steady state temperature reached by our system.

The chosen mesh contains 640.000 control volumes, and it has been refined in areas where the heat transfer is intense. The numerical simulation results for the temperature have been compared to the experimental ones to check their precision. Thus, the value of the temperature has been extracted in the same location as the temperature sensors are located.

Figures 5, 6 and 7 show an overview of the temperature reached by our system in a steady state, such as the temperature measured numerically at the location of the sensors. All the results have a reliable agreement with the experimental ones. The numerical temperature curves display the same behaviour as the experimental ones, and the temperature of the sensors are in good agreement with the experiments:

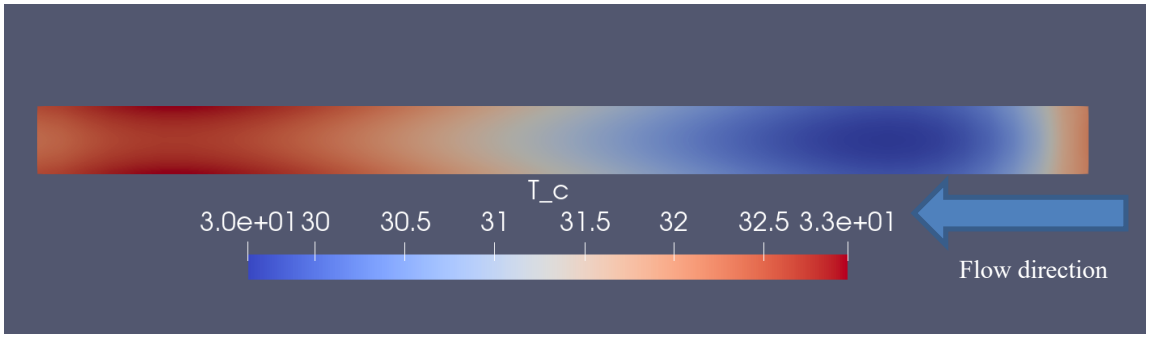

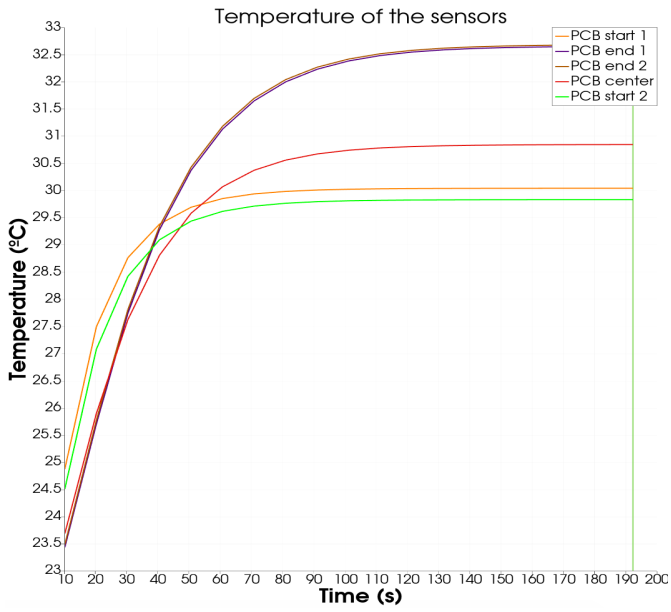

Fig. 5: HTF 17ºC case. (Top) Steady state temperature profile behind the PCB. (Bottom) Temperature of the sensors over time.

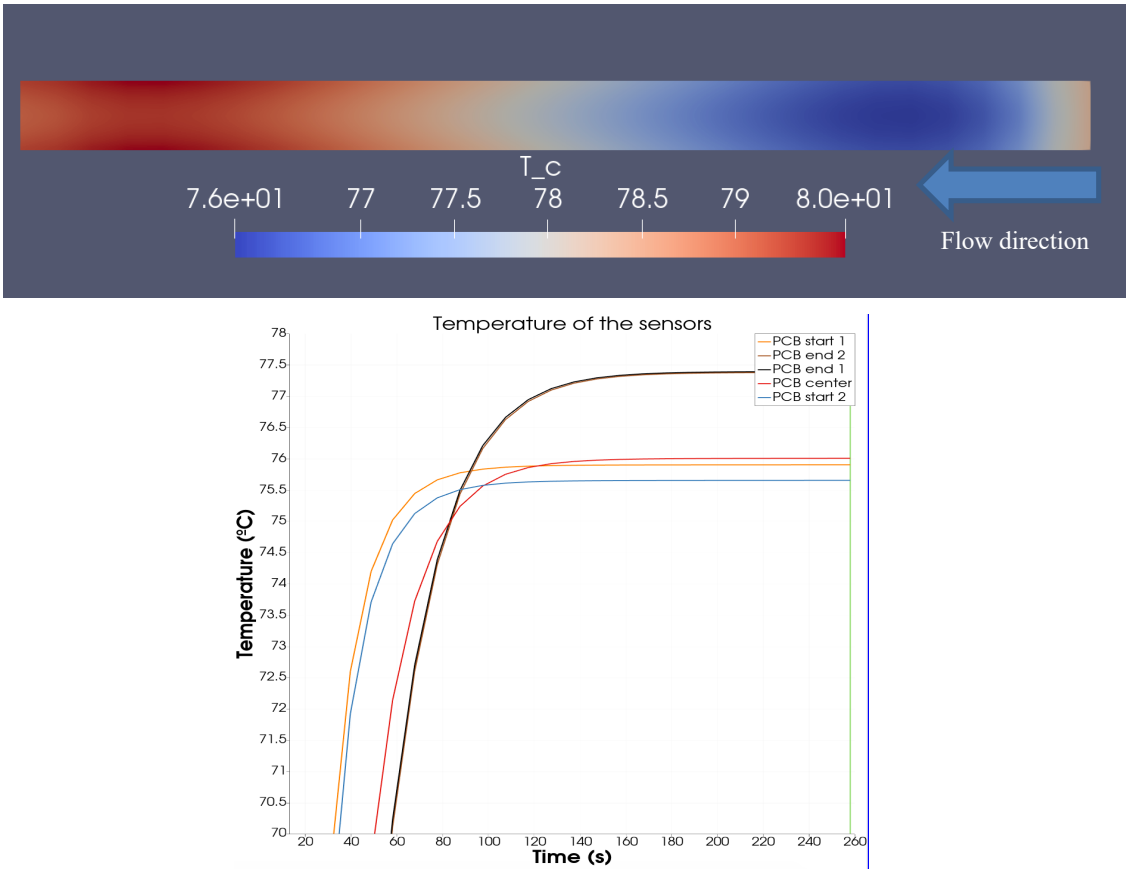

Fig. 6: HTF 65ºC case. (Top) Steady state temperature profile behind the PCB. (Bottom) Temperature of the sensors over time.

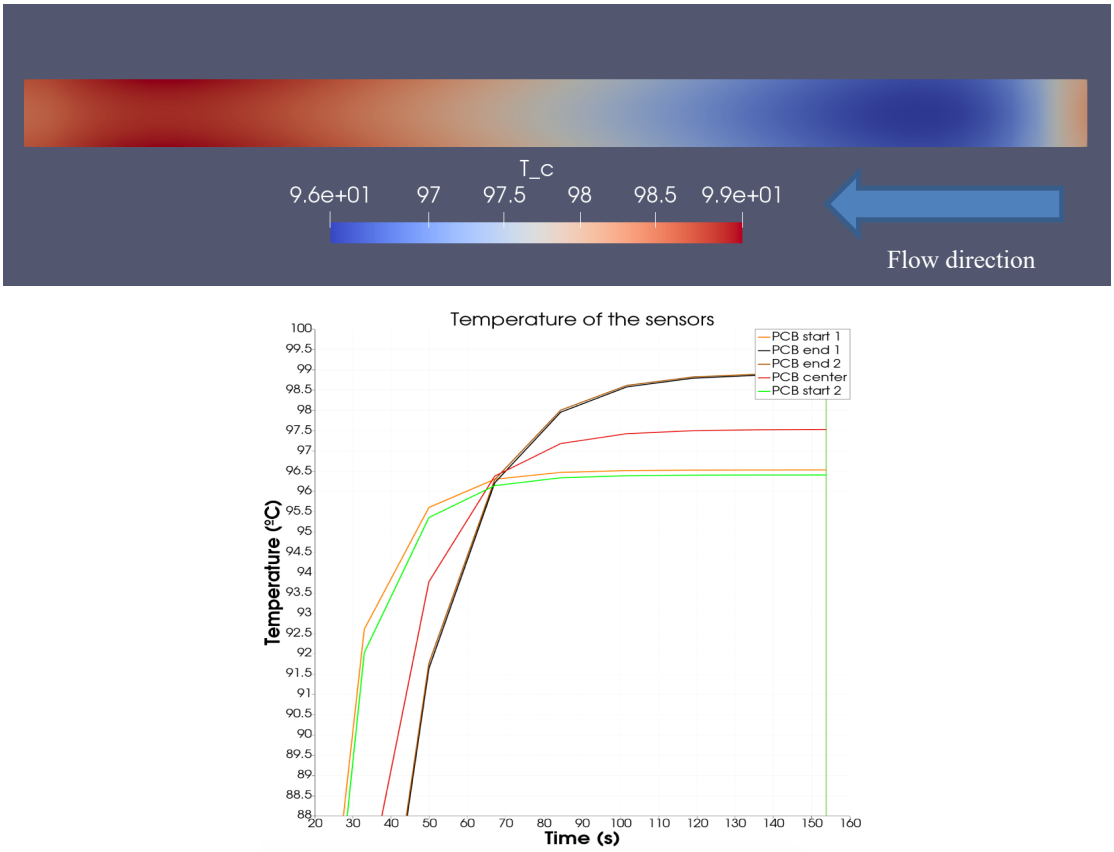

Fig. 7: HTF 90ºC case. (Top) Steady state temperature profile behind the PCB. (Bottom) Temperature of the sensors over time.

A short orange region can be found at the HTF entry of each solid region. This effect is caused by the heat transfer from the pipe to the PCB, and it was also observed by the experiments. Radiation also warms up the solid pipe, and part of this heat is transferred to the PCB.

Tab. 1: Comparison between experimental data and numerical results (steady-state). The temperatures shown in the table are the maximum temperatures measured by the sensors.

	Experimental data	Numerical results
HTF 17ºC	33ºC	32.6ºC
HTF 65ºC	75ºC	77ºC
HTF 90ºC	98.4ºC	98.9ºC

As we can see in the table 1, a very good agreement is found between experimental sensor temperature and the numerical one. Assuming the experimental data is correct, the maximum error (2.7%) is found in the HTF 65ºC. Thus, the model is showing robustness not also under lab conditions but also under real conditions.

4. Towards new geometries

Once the model has been proved to produce good results, this model is going to be used to try new pipe geometries. The main idea of changing the geometry of the pipe (or adding fines) is to increase the heat transfer rate from the pipe to the fluid. Thus, the PCB is reducing its temperature while the fluid is absorbing more heat. Again, the code used to perform the simulations is going to be OpenFOAM. The two pipe designs we are going to test consists of a semicircular pipe with fins. These models and the meshes are described in figures 8 and 9:

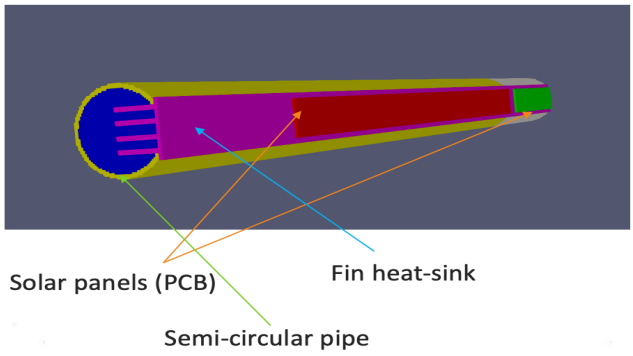

Fig. 8: Mesh used to solve the Fin-Heatsink case.

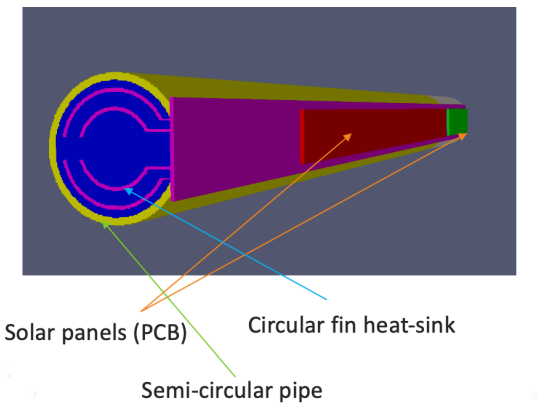

Fig. 9: Mesh used to solve the circular Fin-Heatsink case.

We have results for the previous cases (HTF 17ºC, HTF 65ºC and HTF 90ºC). These results will allow us to compare if these new designs could be more optimum than the previous one. Table 2 shows us a comparison between the temperature measured by the sensors of the previous case (circular pipe) and these new designs:

Tab. 2: Comparison between numerical results obtained for both cases. The temperatures shown in the table are the maximum temperatures measured by the sensors.

	Base case	**Fin heatsink case**	**Circular fin heatsink case**
HTF 17ºC	32.6ºC	25ºC	26.5ºC
HTF 65ºC	77ºC	72.5ºC	73.9ºC
HTF 90ºC	98.9ºC	94.6ºC	95ºC

A decrease of around 4.3ºC – 7.6ºC in the maximum PCB sensor temperature can be seen using a fin heatsink pipe. Table 3 show the average temperature of the back part of the PCB:

Tab. 3: Comparison between numerical results obtained for both cases. The temperatures shown in the table are the average temperature of the back part of the PCB.

	Base case	**Fin heatsink case**	**Circular fin heatsink case**
HTF 17ºC	31.3ºC	23.9ºC	24.3ºC
HTF 65ºC	76.5ºC	71.4ºC	71.8ºC
HTF 90ºC	97.8ºC	93.8ºC	93.9ºC

We can also observe that the fin heatsink seems to work slightly better than the circular fin heatsink within this fluid regime. The explanation for this phenomenon can be explained observing that the maximum heat transfer rate is happening in the fluid region near the PCB, causing the fin-solid part which is further of the PCB to be almost at the fluid temperature. These are good news due to the fact that circular fins are more difficult to manufacture than regular ones (and they are also more expensive).

Furthermore, as the HTF temperature is increased, the maximum PCB temperature reduction is decreased. However, it is still a significant temperature reduction.

In order to quantify the efficiency of the cooling part of the CPVT solar cell, we can define the following quantity:

$$U = \frac{G_b}{\Delta T}, \qquad \text{(eq. 6)}$$

$$\Delta T = \frac{(T_{pV} - T_{in}) - (T_{pV} - T_{out})}{ln\frac{(T_{pV} - T_{in})}{(T_{pV} - T_{out})}}, \qquad \text{(eq. 7)}$$

where T_{pV} is the average temperature at the back part of the PCB, T_{in} is the temperature of the flow at the entrance of the PCB and T_{out} is the temperature of the flow at the exit of the PCB. Observe that this coefficient U provides information about the efficiency of the heat exchange between the PCB and the water flow: the higher the coefficient, the more efficient is the heat exchange, hence, the cooling process.

Tab. 4: Heat transfer coefficient U and pressure drop per meter obtained for the different cases and geometries.

	U HTF 17ºC	U HTF 65ºC	U HTF 90ºC	Pressure drop per meter
Base case	63.3	73.7	77.8	16.4
Fin heatsink case	162.0	152.4	154.5	73.1
Circular fin heatsink case	155.4	146.0	148.7	96.2

As we can see in table 4, the heat transfer coefficient obtained in the fin heatsink cases is almost 2.5 times the heat transfer coefficient of the base case. Furthermore, we can observe that the heat transfer coefficient seems to increase with temperature while this is not happening for the fin heatsink cases. This could explain why the difference of average temperatures seem to decrease while the HTF temperature is increasing. Furthermore, the pressure drop per meter of the fin heatsink case is slightly lower than for the circular fin heatsink case. All these results seem to point out that the fin heatsink will perform better than the circular fin heatsink.

5. Conclusions

A whole and detailed numerical model for CPVT systems has been numerical developed, verified and experimentally tested under different tests conditions. The numerical tool is going to demonstrate an excellent capability of prediction the thermal behaviour of the system, but also as a design tool to develop an optimum configuration for specific solar cooling application. Besides, deep studies must be done in order to optimize the heat absorption. Within this work line, an optimization process to find the optimal number and distances between fins must be carried out.

6. Acknowledgments

This project has received funding from SOLAR-ERA.NET Cofund 2 joint call undertaking under the European Union’s Horizon 2020 research and innovation programme.

7. References

Castro, J., Rigola, J., Kizildag, D., Oliet, C., 2021, Preliminary assessment of a polygeneration system based on a concentrated photovoltaic thermal (CPVT) solar collectors, ISHPC 2021: proceedings, Technische Universität Berlin Campus Charlottenburg, pp. 176-180.

Colomer, G., 2006, Numerical methods for radiative heat transfer, PhD thesis, Universitat Politècnica de Catalunya (UPC), Terrassa.

Buchroithner, A., Gerl, B., Felsberger, R., Wegleiter, H., 2021, Design and operation of a versatile, low-cost, high-flux solar simulator for automated CPV cell and module testing, Solar Energy, Volume 228, Pages 387-404, ISSN 0038-092X.

Felsberger, R., Buchroithner, A., Gerl, B., Wegleiter, H., 2020. Conversion and Testing of a Solar Thermal Parabolic Trough Collector for CPV-T Application, Energies, 13, 6142, 1-24.

Felsberger, R., Buchroithner, A., Gerl, B., Schweighofer, B., Wegleiter, H., 2021, Design and testing of concentrated photovoltaic arrays for retrofitting of solar thermal parabolic trough collectors, Applied Energy, Volume 300, 117427, ISSN 0306-2619.

Guadamund, E., Chiva, J., Colomer, G., Farnós, J., Al Mers, A., Rigola, J., Perez, C., 2017, Development of a high accurate numerical platform for the thermal and optical optimization of linear Fresnel receivers, ISES Solar World Congress/IEA SHC Solar Heating and Cooling Conference, pp. 2000 – 2011.

Sharaf, O. Z., Orhan, M. F., 2015. Concentrated photovoltaic thermal (CPVT) solar collector systems: Part I – Fundamentals, design considerations and current technologies. Renewable and Sustainable Energy Reviews. Volume 50, 1500-1565

Wang, B., 2020, OpenFOAM fvDOM Model discretization notes (URL: https://boyaowang.github.io/boyaowang_OpenFOAM.github.io/2020/09/30/fvdom/). Last access: 08/10/2021.

Zarza, E., 2015, Sesión 13: Diseño de captadores y de campos de captadores cilindroparabólicos, lecture notes, Electricidad Termosolar, Escuela de Organización Industrial, delivered in 2015-2016. URL: (https://www.eoi.es/es/savia/publicaciones/25357/electricidad-termosolar-captadores-cilindroparabolicos-sesion-13-y-14). Last access: 08/10/2021.